PHYSICAL REVIEW E **94**, 040102(R) (2016)

# Direct calculation of the critical Casimir force in a binary fluid

Francesco Puosi, David Lopes Cardozo, Sergio Ciliberto, and Peter C. W. Holdsworth*
*Université de Lyon, Laboratoire de Physique, École normale supérieure de Lyon, CNRS, UMR5672, 46 Allée d'Italie, 69364 Lyon, France*
(Received 25 March 2016; published 21 October 2016)

We show that critical Casimir effects can be accessed through direct simulation of a model binary fluid passing through the demixing transition. We work in the semi-grand-canonical ensemble, in slab geometry, in which the Casimir force appears as the excess of the generalized pressure, $P_\perp - n\mu$. The excesses of the perpendicular pressure, $P_\perp$, and of $n\mu$, are individually of much larger amplitude. A critical pressure anisotropy is observed between forces parallel and perpendicular to the confinement direction, which collapses onto a universal scaling function closely related to that of the critical Casimir force.

DOI: 10.1103/PhysRevE.94.040102

The critical Casimir [1,2] effect makes a major contribution to nanoscale confinement forces [3]. Its contribution is felt as a fluid is driven through the critical ordering transition of an internal degree of freedom, such as the $\lambda$ transition in liquid helium [4] or the demixing transition of a binary fluid [5,6]. It has been measured in wetting films as they pass close to the critical end point for ordering on the liquid gas interface [4,5] or through the fluctuation spectra of colloids as their solvent is driven through the demixing transition [6]. Being a critical phenomenon the Casimir effect is characterized by a universal scaling function [7], which can be extracted with accuracy from the relevant lattice spin model, relying on the thermodynamic relationship between generalized force and derivative of the free energy [8–12]. Universality and thermodynamics allow for this dichotomy but restricts the simulations to average values of the force. Direct simulation of the Casimir force in a fluid [13] or model magnet [14] is a much tougher problem, but accessing it would open the door to instantaneous measurement, microscopic study of the coupling between density correlations, and the critical degrees of freedom, as well as to nonequilibrium effects.

In this letter we present results showing that universal critical Casimir effects, including a pressure anisotropy and the critical Casimir force, can be accessed through direct simulation of such a binary fluid in an anisotropic cell of volume $V = L_\parallel^2 L_\perp$, $L_\perp \ll L_\parallel$; see Fig. 1. We study a fluid mixture of species $A$ and $B$ [15–18] in the semi-grand-canonical ensemble (SGC) [15,16]. Here one imposes $V$, total number of particles $N = N_A + N_B$, temperature $T$, and chemical potential difference, $\mu_{AB} = (\mu_A - \mu_B)/2$, conjugate to the thermally averaged particle difference, $\Delta N = \langle N_A - N_B \rangle$. The relevant free energy thus reads $\Omega_{\rm sgc}(T,N,V,\mu_{AB})$. The model system shows a demixing transition characterized by the order parameter $m = \frac{\Delta N}{N}$, along a line of critical points in the liquid phase, $(T_C(n), \mu_{AB} = 0)$, as the density $n = \frac{N}{V}$ is varied.

The truncation of the diverging correlation length close to the transition introduces $L_\perp^{-1}$, measured in microscopic units, as a third variable characterizing the transition, alongside $t = \frac{T - T_C}{T_C}$ and $\tilde{h} = \mu_{AB}/k_B T_C$. The singular dependence on $L_\perp$ then leads to the Casimir force [2]. To maintain $T_C(n)$ constant so that $t$ is constant along an isotherme, volume changes must be made at constant density. A similar constraint applies for a magnetic system where volume changes occur in a magnetically homogeneous medium [8–10]. Hence, the SGC is thermodynamically equivalent to an Ising model if volume changes are accompanied by changes in $N$. The fundamental thermodynamic relationship then becomes

$$d\Omega_{\rm sgc} = -SdT - (P - \mu n)dV - \Delta N d\mu_{AB}, \qquad (1)$$

with $n$ held constant, where the chemical potential $\mu = (\mu_A + \mu_B)/2$. From this, one can see that the critical Casimir force should manifest itself in the system size dependence of the generalized pressure, $\tilde{P} = P - \mu n$, conjugate variable to volume changes at fixed $n$, rather than the pressure itself [19].

Equation (1) must be generalized further to allow for the development of anisotropies when changing $L_\perp$ and $L_\parallel$ in slab geometry. This allows independent definitions for the pressure measured perpendicular and parallel to the confinement direction [9,19]:

$$P_\perp = -\frac{1}{L_\parallel^2}\frac{\partial \Omega_{\rm sgc}}{\partial L_\perp}\bigg|_N, \quad P_\parallel = -\frac{1}{2L_\perp L_\parallel}\frac{\partial \Omega_{\rm sgc}}{\partial L_\parallel}\bigg|_N, \qquad (2)$$

and for the generalized pressure $\tilde{P}_\perp = P_\perp - \mu n$ and $\tilde{P}_\parallel = P_\parallel - \mu n$.

For a macroscopic sample one finds $\Omega_{\rm sgc} = k_B T V \omega_{\rm bulk}(T,n,\mu_{AB})$, where $\omega_{\rm bulk}$ is the dimensionless free-energy density, so that $P_\perp = P_\parallel = P = -k_B T \omega_{\rm bulk}$, the bulk pressure. In slab geometry, with $L_\perp$ on a mesoscale, corrections to bulk thermodynamics give the announced extra $L_\perp$ dependence; $\Omega_{\rm sgc} = k_B T(\omega_{\rm bulk} + \omega_{\rm ex}(L_\perp))$, where $\omega_{\rm ex}(L_\perp)$ is the excess free energy [7,20,21]. Hence, one finds excess values for all thermodynamic quantities, including pressure, both perpendicular *and* parallel to the confinement direction, internal energy density, $u_{\rm ex}$, and chemical potential, $\mu_{\rm ex}$.

Near the demixing transition there is a critical contribution to the excess free energy, $\omega_{\rm ex}^s$, modifying the singular part of the free energy, $\omega^s(t,\tilde{h},L_\perp) = \omega_0^s(t,\tilde{h}) + \omega_{\rm ex}^s(t,\tilde{h},L_\perp)$, where $\omega_0^s$ is the value in the bulk.

This, however, is not the only contribution to the excess. Regular surface terms, coming, for example, from Van der Waals interactions and leading to a surface free energy [22,23], also make important contributions that can be taken into

*peter.holdsworth@ens-lyon.fr

 

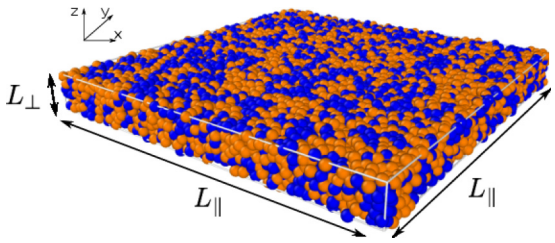


FIG. 1. Typical configuration for the binary fluid in slab geometry. Particles of type A (blue) and type B (orange). The image is shown for density $n = 0.7$ and dimensions $L_\perp = 5$ and $L_{||} = 60$; see text.

account both experimentally [4] and numerically [10]. In the present work they are minimized as we use periodic boundaries, but even here, the incommensurability of the pair correlation function with the boundaries leads to noncritical contributions [24].

The critical excess free energy has universal scaling properties that are at the root of all critical phenomena in a finite system [25]. Limiting here to the temperature axis one finds

$$\omega^s_{\rm ex}(t, L_\perp) = L_\perp^{-d}\Theta(x_t), \quad x_t = t\left(\frac{L_\perp}{\xi_0^+}\right)^{1/\nu}, \tag{3}$$

where $\xi_0^+$ is a nonuniversal amplitude that depends on $n$, which can be estimated from the small wavelength part of the density structure factor [16,19,26].

The critical confinement force per unit area, perpendicular (parallel) to the confinement axis, is the critical contribution to the excess of $\tilde{P}_{\perp(\|)}$,

$$\begin{aligned} f_\perp^c &= (\tilde{P}_\perp)^s_{\rm ex}/k_BT = L_\perp^{-d}\theta(x_t), \\ f_\parallel^c &= (\tilde{P}_\parallel)^s_{\rm ex}/k_BT = -L_\perp^{-d}\Theta(x_t), \end{aligned} \tag{4}$$

with

$$\theta(x_t) = (d-1)\Theta(x_t) - \frac{x_t}{\nu}\frac{\partial\Theta}{\partial x_t}\bigg|_{\tilde{h}}. \tag{5}$$

The critical Casimir force, in units of $k_BT$, is $f_\perp^c$. Calculation of $\mu_{\rm ex}$ can be bypassed by studying the pressure anisotropy, as the chemical potential is intrinsically isotropic, so that $\tilde{P}_\perp - \tilde{P}_\parallel = P_\perp - P_\parallel$. This is pure excess and the critical contribution to it takes the universal form

$$f_\perp^c - f_\parallel^c = L_\perp^{-d}[\theta(x_t) + \Theta(x_t)]. \tag{6}$$

Using Eq. (5), the function $\Theta$ can be calculated from $\theta$ and vice versa [27], so that both functions can be extracted with precision from simulations of the Ising model [8,19].

We have tested these ideas using a fluid of A and B particles, interacting via a smoothly truncated potential: $v(r) = \phi(r) - \phi(r_c) - (r - r_c)\frac{d\phi}{dr}|_{r=r_c}$ for $r \leqslant r_c$, where $\phi(r)$ is the Lennard-Jones interaction, $\phi(r) = 4\epsilon_{\alpha\beta}[(\sigma_{\alpha\beta}/r)^{12} - (\sigma_{\alpha\beta}/r)^6]$ between species $\alpha,\beta$ separated by distance $r$ [28]. We take a symmetric mixture of equal mass $m$, with $\sigma_{AA} = \sigma_{BB} = \sigma_{AB} = \sigma, \epsilon_{AA} = \epsilon_{BB} = 2\epsilon_{AB} = \epsilon, r_c = 2.5\sigma$ and take $\epsilon$, $\sigma$, $m$, and $\tau_0 = \sigma\sqrt{(m/\epsilon)}$ as the units of energy, length, mass, and time, respectively.

We performed hybrid molecular dynamics (MD) and metropolis Monte Carlo (MC) simulations (using LAMMPS [29]) in slab geometry of width $L_\parallel = 60$ and thickness $L_\perp = 5$ and 6 with periodic boundaries (see Fig. 1 for a typical setup). These are thin films that at first sight appear far from the three-dimensional scaling limit. However, the crossover from two- to three-dimensional criticality occurs for surprisingly small film width [30], allowing three-dimensional scaling to a reasonable approximation for this range of thickness. The lateral size, $L_\parallel$, is sufficiently large to place us in the scaling limit for slab geometry [9,10,19]. The equations of motion were integrated using the velocity Verlet algorithm with a time step $\delta t = 10^{-5}$. Constant temperature was achieved using a Nosé-Hoover thermostat [31]. Particle identity switches were made using MC, with a sweep of attempted changes made every $10^3$ MD steps. At each temperature we started from an equilibrium configuration of $A$ particles and equilibrated for at least $3 \times 10^7$ MD steps.

The pressure $P_k$ in direction $k = x$, $y$, or $z$ can be accessed by the Virial formula [32], from which we define the pressure anisotropy:

$$P_\perp - P_\parallel = P_z - \frac{P_x + P_y}{2}. \tag{7}$$

The interaction part of the chemical potential was calculated using the Widom insertion method [32,33], which was adapted to the SGC with $\mu_{AB} = 0$ by inserting either a virtual $A$ or virtual $B$ particle at random.

The model has been benchmarked in detail for $n = 1$ and $\mu_{AB} = 0$, showing a second order demixing transition within the dense liquid phase at $T = 1.4230 \pm 0.0005$ [16]. We anticipate from previous studies that for this parameter set the phase transition continues along a line of critical points in the $n - T$ plane, intercepting the gas phase at a tricritical point [34], which we avoid by working at sufficiently high densities, $n \geqslant 0.6$.

In Fig. 2 we show the pressure anisotropy for $n = 0.6$ and $n = 0.7$ for $L_\perp = 5$ and $L_\perp = 6$ in the region of the transition. The transition temperatures, $T_C(n = 0.6) = 1.18 \pm 0.01$, $T_C(n = 0.7) = 1.32 \pm 0.01$ were estimated from the susceptibility maximum of a cubic system of size, $L_\perp = L_{||} = 32$, which for the values of $L_\perp$ and precision attained here can be considered as the bulk transition temperatures. Figures 2(a) and 2(b) show the raw data as a function of temperature, which illustrate both a critical effect through the transition and a noncritical contribution, resulting in a nonzero value for the anisotropy far from the transition.

The existence of a noncritical pressure anisotropy for systems confined on this scale [24] is illustrated explicitly in Fig. 2(c), where we show data for a single component Lennard-Jones fluid with energy and length scales $\epsilon$ and $\sigma$ for $n = 0.6$ in the same temperature range. Away from the transition the anisotropy for the binary and simple fluids are of similar magnitude. As an ansatz for the noncritical contribution, to be subtracted from the total anisotropy, we take

$$P_{\rm nc}(L_\perp, n, T) = A_{\rm nc}(L_\perp, n) + B_{\rm nc}(L_\perp, n)|m|, \tag{8}$$

where $m$ is the order parameter for the transition, measured during the simulation and $A_{\rm nc}(L_\perp, n)$ and $B_{\rm nc}(L_\perp, n)$ are

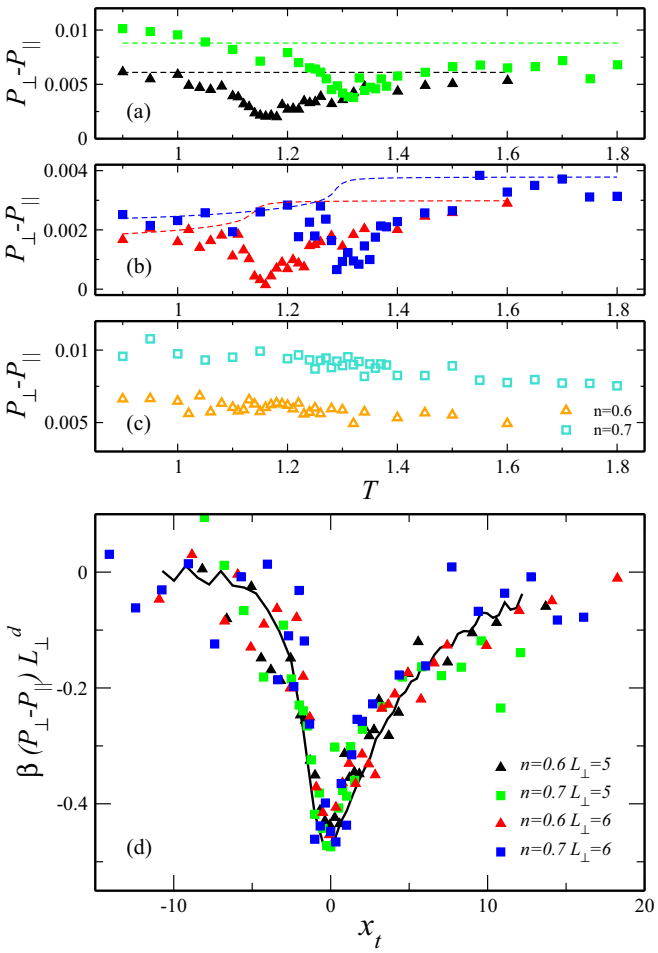


FIG. 2. (a) pressure anisotropy $P_\perp - P_{||}$ in slab geometry with $L_\perp = 5$ for $n = 0.6,0.7$. Dashed lines mark the noncritical pressure anisotropy, estimated from the high and low pressure limits and using Eq. (8); see text. (b) pressure anisotropy and estimated noncritical pressure anisotropy for $L_\perp = 6$. (c) pressure anisotropy for a one component Lennard-Jones fluid for $L_\perp = 5$; see text. (d) finite-size scaling of the critical part of the pressure anisotropy for the systems in (a) and (b). Data are compared to an estimate of the universal scaling function $\theta + \Theta$ computed from a simulation of an Ising model (solid line) with $L_\perp = 9$ and 20 and $L_{||} = 60$ [19].

constants estimated from the high and low temperature values for the data shown in Figs. 2(a) and 2(b). This represents the pressure anisotropy of an effective single component fluid whose characteristics evolve as the composition of the binary fluid evolves through the transition. The amplitude of this evolution is fitted, but the rate, as a function of temperature is fixed by the evolution of $m$, which is determined numerically. For $L_\perp = 5$ it was sufficient to set $B_{\rm nc} = 0$, giving a constant shift shown by the dashed line in Fig. 2(a). For $L_\perp = 6$ both constants were taken to be nonzero with the resulting shift functions shown in Fig. 2(b). The amplitude of this correction is reduced on going from $L_\perp = 5$ to $L_\perp = 6$, as expected, as being noncritical, it should fall exponentially to zero as $L_\perp$ increases [24].

Removing the noncritical contribution gives an estimate for the critical reduced pressure anisotropy, plotted against $x_t$ in Fig. 2(d), with the estimated amplitudes $\xi_0^+(n = 0.6) = 0.46 \pm 0.04$ and $\xi_0^+(n = 0.7) = 0.55 \pm 0.04$ The fluid data indeed collapses, within statistical error onto a single master curve constructed from simulations of the Ising model [19]. This function shows a minimum value just below but close to the transition, with an overall form similar to $\theta(x_t)$. The contribution from the excess free energy generates a broader function, particularly above the transition and gives a depth at $T = T_C$, which is 3/2 that of $\theta(x_t)$ [19].

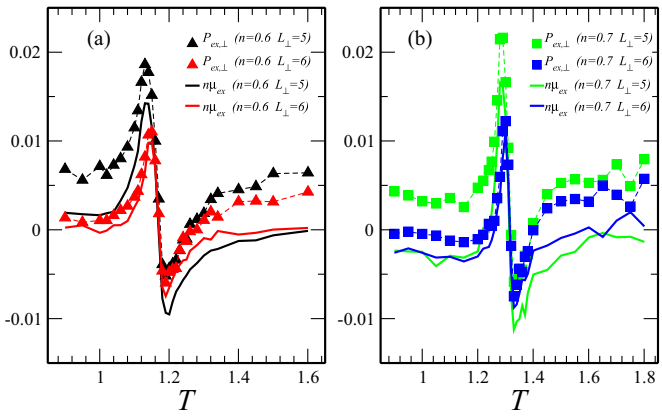


FIG. 3. Excess part of the confinement pressure $P_{\rm ex,\perp}$ (symbols), and excess chemical potential multiplied by the density, $n\mu_{\rm ex}$ (lines), for $L_\perp = 5,6$ and $n = 0.6$ (a) and $n = 0.7$ (b).

Given the small values for $L_\perp$, one can expect the results to be subject to corrections to scaling. These are relatively small for spin systems with periodic boundaries [10,35–37]. The incommensurability of the pair correlation function through the boundaries constitutes a contribution to these corrections, which is specific to a binary fluid. The smallness of the other corrections, compared, for example, with open or fixed boundaries [10], provides a convenient test for our procedure.

In Fig. 3 we show the excess values for the pressure measured perpendicular to the confinement direction, $P_{\rm ex,\perp} = P_\perp - P^{\rm cubic}$, and for the product of density and chemical potential, $n\mu_{\rm ex} = n\mu - n\mu^{\rm cubic}$. The quantities $P^{\rm cubic}$ and $\mu^{\rm cubic}$ were estimated from the cubic sample with $L_\perp = L_{||} = 32$, which we consider as the bulk values [9,19]. The first thing to notice is that these two quantities exhibit a sharply varying alternating function through the transition, similar in form to the excess internal energy [19,25] but radically different from the Casimir function exposed by the pressure anisotropy. Second, comparing with Figs. 2(a) and 2(b), one can see that the amplitude of these excess quantities is an order of magnitude bigger than that expected for the Casimir force for $L_\perp = 5$ and 6. These measurements then confirm the thermodynamics presented above: in the SGC ensemble the Casimir force is related to the excess of $\tilde{P}_\perp$ rather than the pressure itself. Its direct calculation poses the numerical challenge of resolving this small signal from the difference between these two quantities.

In Figs. 4(a) and 4(b), we show $\tilde{P}_{\rm ex,\perp}$ versus $T$ for $L_\perp = 5,6$ and $n = 0.6$ and $n = 0.7$, respectively, constructed from the data shown in Fig. 3. The raw data shown in Figs. 4(a) and 4(c) fluctuates around values that are of the correct order of magnitude for the Casimir force but its observation is obscured by what again we interpret as a

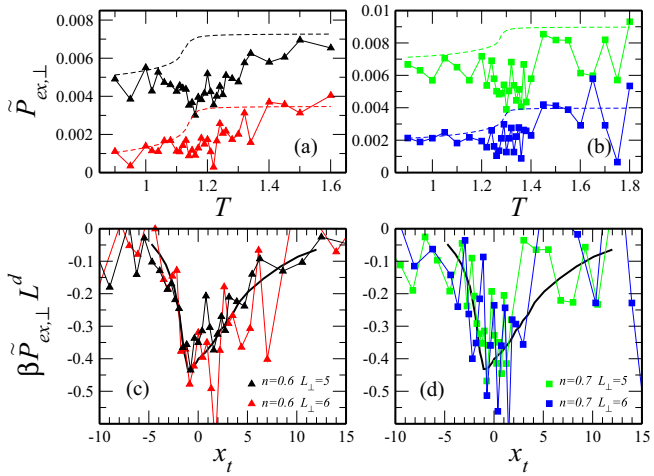


FIG. 4. (a, b) Symbols correspond to the excess part of the generalized pressure $\tilde{P}_{\mathrm{ex},\perp}$ with $L_\perp = 5,6$ and for $n = 0.6$ (a) and $n = 0.7$ (b). Dashed lines are estimates of the noncritical part of $\tilde{P}_{\mathrm{ex},\perp}$. (c, d) Scaling of $\tilde{P}_{\mathrm{ex},\perp}$ and the scaling function $\theta(x_t)$ obtained from Ising model simulation in Ref. [8] (full line).

noncritical contribution, $\tilde{P}_{\mathrm{nc}}(L_\perp, n, T)$. We model $\tilde{P}_{\mathrm{nc}}$ using the functional form of Eq. (8). The results are superimposed on Figs. 4(a) and 4(b). In each case the constants $A$ and $B$ were fixed by estimating the asymptotes at high and at low temperature. The subsequent data collapse, once $\tilde{P}_{\mathrm{nc}}$ has been subtracted, is shown in Figs. 4(c) and 4(d) and compared with the universal function, as estimated from simulations of the Ising model [8]. The data is extremely noisy and the process is clearly somewhat exploratory, but despite this it seems clear that the universal function is emerging from the simulation data for the binary mixture.

In conclusion, we have shown that one can access Casimir effects directly from simulations of a binary fluid undergoing a critical demixing transition. We worked in the SCG ensemble as it is thermodynamically equivalent to the Ising model and because it offers an accessible route to direct simulation in a fluid system. Measurement of the pressure anisotropy, $P_\perp - P_\parallel$ yields a universal scaling function intimately related to the critical Casimir force, while direct calculation of the force requires the excess of the generalized pressure $\tilde{P}_\perp = P_\perp - n\mu$. Resolving a signal from the difference between these already highly fluctuating quantities proved to be at the limit of our computing resources. In particular, obtaining data for $\mu$ of high quality was extremely time consuming and the key to future improvements is the development of more efficient algorithms for estimating $\mu$.

An alternative to our approach would be to work in the grand canonical ensemble [13,17,34]. In this case, as the chemical potential fixes the average density during a volume change, the Casimir force should come directly from the excess pressure exerted on the confining walls. However, simulating density fluctuations is time consuming, making high-quality data collection difficult. As a consequence, calculation of the pressure anisotropy and other excess quantities such as the internal energy are more straightforward in the SGC. For the Casimir force, things are less clear and in the light of the results presented here it would certainly be interesting to explore grand canonical simulations further. The pressure anisotropy exposed here could, in principle, be extracted from spin models using the methods proposed in Ref. [14] and it would also be of interest to pursue this issue in future work.

Making direct simulations of a binary fluid has highlighted the existence of the pressure anisotropy associated with confinement; a rather unusual situation for an otherwise isotropic fluid. This anisotropy could in principle be measured experimentally and we hope that our work will stimulate the development of protocols for this. One possible avenue could be through the evolution of the forces between arrays of colloidal particles pinned in anisotropic geometries, immersed in a binary fluid as it passes through the demixing transition.

Finally, the most compelling motivation for making direct simulations in a fluid system is that it allows the study of both universal properties and microscopic processes. The use of molecular dynamics gives access to real dynamical processes and will open the door to studies of nonequilibrium processes. In this paper, we have been limited to periodic boundaries, but while more realistic boundaries will require increased computing power and efficiency, there is no theoretical barrier to the study of fixed, or open boundaries, corresponding to experimental setups. Future experiments will certainly move from detailed studies of Casimir forces in equilibrium situations to the study of nonequilibrium phenomena. Numerical simulations of model fluid systems such as those presented here will play an important role in understanding these exciting developments.

*Note added in proof.* We recently became aware of the following submission [38] which uses the same model to study related concepts.

We thank J.-L. Barrat and A. C. Maggs for useful discussions. This work was financed by the ERC Grant OUTEFLUCOP and used the numerical resources of the PSMN at the ENS Lyon. P.C.W.H. acknowledges financial support from ANR Grant FISICS.

[1] H. Casimir, On the attraction between two perfectly conducting plates, Proc. R. Neth. Acad. Arts Sci. **51**, 793 (1948).

[2] P.-G. de Gennes and M. E. Fisher, Phénomènes aux parois dans un mélange binaire critique, C. R. Acad. Sci. Paris Ser. B **287**, 207 (1978).

[3] A. Gambassi, The Casimir effect: From quantum to critical fluctuations, J. Phys.: Conf. Ser. **161**, 012037 (2009).

[4] A. Ganshin, S. Scheidemantel, R. Garcia, and M. H. W. Chan, Critical Casimir Force in $^4$He Films: Confirmation of Finite-Size Scaling, Phys. Rev. Lett. **97**, 075301 (2006).

[5] M. Fukuto, Y. F. Yano, and P. S. Pershan, Critical Casimir Effect in Three-Dimensional Ising Systems: Measurements on Binary Wetting Films, Phys. Rev. Lett. **94**, 135702 (2005).

[6] C. Hertlein, L. Helden, A. Gambassi, S. Dietrich, and C. Bechinger, Direct measurement of critical Casimir forces, Nature **451**, 172 (2008).

[7] M. Krech, *The Casimir Effect in Critical Systems* (World Scientific, Singapore, 1994).

[8] D. Lopes Cardozo, H. Jacquin, and P. C. W. Holdsworth, Critical Casimir forces in a magnetic system: An experimental protocol, Phys. Rev. B **90**, 184413 (2014).

[9] A. Hucht, D. Grüneberg, and F. M. Schmidt, Aspect-ratio dependence of thermodynamic Casimir forces, Phys. Rev. E **83**, 051101 (2011).

[10] O. Vasilyev, A. Gambassi, A. Maciolek, and S. Dietrich, Universal scaling functions of critical Casimir forces obtained by Monte Carlo simulations, Phys. Rev. E **79**, 041142 (2009).

[11] O. A. Vasilyev and S. Dietrich, Critical Casimir forces for films with bulk ordering fields, Europhys. Lett. **104**, 60002 (2013).

[12] M. Hasenbusch, Thermodynamic Casimir effect for films in the three-dimensional Ising universality class: Symmetry-breaking boundary conditions, Phys. Rev. B **82**, 104425 (2010).

[13] N. B. Wilding and M. Krech, Effect of criticality on wetting layers: A Monte Carlo simulation study, Phys. Rev. E **57**, 5795 (1998).

[14] D. Dantchev and M. Krech, Critical Casimir force and its fluctuations in lattice spin models: Exact and Monte Carlo results, Phys. Rev. E **69**, 046119 (2004).

[15] S. Materniak, A. Patrykiejew, and S. Sokołowski, The phase behavior of two-dimensional symmetrical mixtures, J. Chem. Phys. **133**, 244501 (2010).

[16] S. K. Das, Jürgen Horbach, Kurt Binder, Michael E. Fisher, and Jan V. Sengers, Static and dynamic critical behavior of a symmetrical binary fluid: A computer simulation, J. Chem. Phys. **125**, 024506 (2006).

[17] N. B. Wilding, Continuous demixing at liquid-vapor coexistence in a symmetrical binary fluid mixture, Phys. Rev. E **67**, 052503 (2003).

[18] N. B. Wilding, Critical end point behavior in a binary fluid mixture, Phys. Rev. E **55**, 6624 (1997).

[19] David Lopes Cardozo, Finite size scaling and the critical Casimir force: Ising magnets and binary fluids, Ph.D. thesis, École normale supérieure de Lyon, 2015.

[20] Nigel Goldenfeld, *Lectures on Phase Transitions and the Renormalization Group*, Advanced Book Program (Addison-Wesley, Reading, Mass., 1992).

[21] A. Gambassi, A. Maciołek, C. Hertlein, U. Nellen, L. Helden, C. Bechinger, and S. Dietrich, Critical Casimir effect in classical binary liquid mixtures, Phys. Rev. E **80**, 061143 (2009).

[22] I. E. Dzyaloshinskii, E. M. Lifshitz, and L. P. Pitaevskii, The general theory of van der waals forces, Adv. Phys. **10**, 165 (1961).

[23] E. Cheng and M. W. Cole, Retardation and many-body effects in multilayer-film adsorption, Phys. Rev. B **38**, 987 (1988).

[24] Minerva González-Melchor, Pedro Orea, Jorge López-Lemus, Fernando Bresme, and José Alejandre, Stress anisotropy induced by periodic boundary conditions, J. Chem. Phys. **122**, 094503 (2005).

[25] Martin Hasenbusch, Specific heat, internal energy, and thermodynamic Casimir force in the neighborhood of the λ-transition, Phys. Rev. B **81**, 165412 (2010).

[26] Subir K. Das, Jürgen Horbach, and Kurt Binder, Transport phenomena and microscopic structure in partially miscible binary fluids: A simulation study of the symmetrical Lennard-Jones mixture, J. Chem. Phys. **119**, 1547 (2003).

[27] H. W. Diehl, D. Grüneberg, M. Hasenbusch, A. Hucht, S. B. Rutkevich, and F. M. Schmidt, Large-*n* approach to thermodynamic Casimir effects in slabs with free surfaces, Phys. Rev. E **89**, 062123 (2014).

[28] M. P. Allen and D. J. Tildesley, *Computer Simulations of Liquids* (Oxford University Press, Clarendon, 1987).

[29] S. Plimpton, Fast parallel algorithms for short-range molecular dynamics, J. Comput. Phys. **117**, 1 (1995).

[30] K. Binder, Monte carlo study of thin magnetic ising films, Thin Solid Films **20**, 367 (1974).

[31] S. Nosé, A unified formulation of the constant temperature molecular dynamics methods, J. Chem. Phys. **81**, 511 (1984).

[32] D. Frenkel and B. Smit, *Understanding Molecular Simulation, Second Edition: From Algorithms to Applications*, 2nd ed. (Academic Press, San Diego, 2001).

[33] B. Widom, Some topics in the theory of fluids, J. Chem. Phys. **39**, 2808 (1963).

[34] N. B. Wilding, F. Schmid, and P. Nielaba, Liquid-vapor phase behavior of a symmetrical binary fluid mixture, Phys. Rev. E **58**, 2201 (1998).

[35] Martin Hasenbusch, Thermodynamic Casimir effect: Universality and corrections to scaling, Phys. Rev. B **85**, 174421 (2012).

[36] Andrea Pelissetto and Ettore Vicari, Critical phenomena and renormalization-group theory, Phys. Rep. **368**, 549 (2002).

[37] Martin Hasenbusch, Finite size scaling study of lattice models in the three-dimensional Ising universality class, Phys. Rev. B **82**, 174433 (2010).

[38] S. Roy, S. Dietrich, and F. Höfling, Structure and dynamics of binary liquid mixtures near their continuous demixing transitions, J. Chem. Phys. **145**, 134505 (2016).